Bulletin of Electrical Engineering and Informatics
Vol. 12, No. 3, June 2023, pp. 1458~1463
ISSN: 2302-9285, DOI: 10.11591/eei.v12i3.4772

The impacts of green $LaBSiO_5$: Tb^{3+}, Ce^{3+} phosphor on lumen output of white LEDs

Ha Thanh Tung[1], Huu Phuc Dang[2], Phung Ton That[3]
[1]Faculty of Basic Sciences, Vinh Long University of Technology Education, Vinh Long, Vietnam
[2]Faculty of Fundamental Science, Industrial University of Ho Chi Minh City, Ho Chi Minh City, Vietnam
[3]Faculty of Electronics Technology, Industrial University of Ho Chi Minh City, Ho Chi Minh City, Vietnam

Article Info

Article history:

Received Sep 13, 2022
Revised Nov 2, 2022
Accepted Nov 27, 2022

Keywords:

Color homogeneity
$LaBSiO_5$
Luminous flux
Monte Carlo theory
WLEDs

ABSTRACT

The traditional solid-state technique was used to create $LaBSiO_5$ phosphors doped with Ce^{3+} and Tb^{3+} at 1,100 °C. These phosphors' phase purity and luminous characteristics are looked at. Under ultraviolet (UV) light stimulation, $LaBSiO_5$: Tb^{3+} phosphors emit bright green light, whereas $LaBSiO_5$ samples incorporated with Ce^{3+} emit blue-violet light. With UV ray stimulation, $LaBSiO_5$ samples incorporated with Ce^{3+} as well as Tb^{3+} emit blue-violet as well as green illumination. The 5d-4f shift for Ce^{3+} is responsible for the blue-violet radiation, while the $^5D_4 \rightarrow {}^7F_5$ transition of Tb^{3+} is responsible for the green radiation. The mechanism for power conversion between Ce^{3+} and Tb^{3+} was examined since there is a spectral overlap among the stimulation line for Tb^{3+} and the emitting line for Ce^{3+}.

Corresponding Author:

Huu Phuc Dang
Faculty of Fundamental Science, Industrial University of Ho Chi Minh City
No. 12 Nguyen Van Bao Street, Ho Chi Minh City, Vietnam
Email: danghuuphuc@iuh.edu.vn

1. INTRODUCTION

In a variety of purposes, including fluorescent lighting, plasma display panels, field emission displays, and white light-emitting diodes, the rare-earth ion Tb^{3+} would be extensively exploited in the form of a trigger in green [1]–[3]. Nevertheless, since *4f-4f* transitions are parity prohibited, Tb^{3+} exhibits faint absorption apexes within the close-under ultraviolet (UV) scope [4]. The sensitizer was co-doped in phosphors to enhance Tb^{3+} absorption. Ce^{3+} not only has strong luminous characteristics with a wide band, but it can also function as a powerful sensitizer [5]. It is capable of effectively absorbing UV radiation and transmitting the energy to the luminous core, increasing the strength of the emission. Numerous phosphors that include Ce^{3+} and Tb^{3+} have been created to efficiently produce green illumination by transferring energy between Ce^{3+} and Tb^{3+} ions [6]. The energy conversion effectiveness between Ce^{3+} and Tb^{3+} ions, for instance, may reach 95% for samples of $Ba_2Y(BO_3)_2Cl$:Ce^{3+}, Tb^{3+} [7], [8].

$LaBSiO_5$ (LBS) is a combination that exhibits exceptional heat and hydrolytic stability and is regarded as a productive host for luminescence [9], [10]. The equivalent lattice constants for LBS's trigonal crystal structure would include *a* value of 6.874 Å, *b* value of 6.874 Å, *c* value of 6.717 Å, Z value of 3, and *V* value of 274.87 $Å^3$. La^{3+} is located at six coordinations with O^{2-} ions in this crystal formation, while BO_4 and SiO_4 would be connected through corner-sharing and create a loop formation with six components. According to Song *et al*. [11], Kustov *et al*. [12] have studied LBS incorporated with Eu^{3+} as well as Ce^{3+}. The luminous characteristics for LBS:Eu^{3+}, Al^{3+} were examined in our most current study [13]. To the greatest of our understanding, no new research on rare earth ion-doped $LaBSiO_5$ has been disclosed. In this work, solid-state reactions were used to synthesize LBS incorporated with Tb^{3+} as well as Ce^{3+}, and the compounds' structures and luminescence characteristics were examined. Lastly, it was looked into how energy moved between Ce^{3+} and Tb^{3+} for LBS.

2. COMPUTATIONAL METHOD

A solid-state reaction was used to create $La_{1-x}BSiO_5$:xTb^{3+} samples (x values of 0.05, 0.10, 0.15, 0.20, and 0.25) La_2O_3 (99.99%), Tb_4O_7 (99.99%), H_3BO_3 (A.R.), and SiO_2 were the initial substances (A.R.). An additional 10% molar stoichiometric quantity of H_3BO_3 was applied to the initial substances to make up for the loss of B_2O_3 [14]. The raw components were combined and pulverized in an agate mortar in stoichiometric quantities. The combinations were then burned for 4 hours in the air at 1,100 °C. The agglomerate was ground to get the phosphors. The preparation of $La_{1-y}BSiO_5$:yCe^{3+} samples (y values of 0.01, 0.02, 0.03, 0.04, 0.05) as well as $La_{0.85-z}BSiO_5$:$0.15Tb^{3+}$, zCe^{3+} (z values of 0.03, 0.05, 0.10, 0.15, 0.25, and 0.35) followed the same steps as for $La_{1-x}BSiO_5$:x Tb^{3+}, with the exception that said specimens would be heated within a decreasing atmosphere with N_2-to-H_2 ratio as 95:5. $LaBSiO_5$ samples incorporated with rare-earth ions had their X-ray diffraction (XRD) patterns examined [15], [16]. The XRD behaviors for the compounds $La_{0.85}BSiO_5$:$0.15Tb^{3+}$, $La_{0.60}BSiO_5$:0.15 Tb^{3+}, as well as $La_{0.50}BSiO_5$:$0.15Tb^{3+}$,$0.35Ce^{3+}$ are shown. Arch a would be said behavior for $La_{0.85}BSiO_5$:$0.15Tb^{3+}$ heated under a temperature of 1100 °C, being compatible with the universal joint committee on powder diffraction standards (JCPDS) card for LBS (JCPDS 87-2172). Such an outcome demonstrates that the samples and LBS both have the similar phase and trigonal crystal structure. The host structure is not significantly altered by the doping of Tb^{3+}, as well as Tb^{3+} ions occupy the location of La^{3+} ions. $La_{0.60}BSiO_5$:$0.15Tb^{3+}$,$0.25Ce^{3+}$ would be the XRD pattern making up curve b; no other apparent phases can be identified [17]. Other phases may be seen via the XRD behavior for $La_{0.50}BSiO_5$:$0.15Tb^{3+}$,$0.35Ce^{3+}$ up to a Ce^{3+} concentration of 0.35.

The excitation as well as discharge spectra for $La_{1-x}BSiO_5$:xTb^{3+} excitation are displayed. The *4f-5d* transition of Tb^{3+} is mostly responsible for the wide band between 270 and 300 nm. The inner-formational *4f-4f* shift for Tb^{3+} are attributed to the strong peaks in the wavelength range of 300 to 390 nm. As the Tb^{3+} concentration rises, the stimulation strengths of the 4f-5d and *4f-4f* conversions of Tb^{3+} become stronger, peaking at 0.15 Tb^{3+} concentration. The emitting spectra for $La_{1-x}BSiO_5$:xTb^{3+} excited at 378 nm are depicted. Owing to the Tb^{3+} $^5D_4 \rightarrow {}^7F_J$ transitions, these phosphors may generate green ray yielding major maxima under 492, 544, 587, as well as 621 nm (J=6, 5, 4, and 3, respectively). Being a magnetic dipole permitted shift having J value of ±1, the highest green emitting peak among them would be under 544 nm ($^5D_4 \rightarrow {}^7F_5$ shift). The emitting strengths likewise rise as the Tb^{3+} concentration grows. Among these five phosphors, $La_{0.85}BSiO_5$:$0.15Tb^{3+}$ exhibits the greatest green radiation. Regards to the emitting spectrum, the CIE hue coordinates of $La_{0.85}BSiO_5$:$0.15Tb^{3+}$ include x value of 0.304 as well as y value of 0.594.

Owing to Dexter and Schulman theory, energy is transferred between a trigger and a different one up to the point of a power sink being achieved within the latticework, which causes concentration abatement in many phosphors. It shows that contact is connected to concentration quenching and that the critical concentration relies on the likelihood of the transference, allowing the assimilated stimulation power to arrive at specific abatement sites. It is possible to calculate the critical range (Rc) for energy transfer using the critical concentration for quenching. The equation can be used to practically compute the Rc values [18].

$$Rc = 2\left(\frac{3V}{4\pi x_c N}\right)^{\frac{1}{3}} \tag{1}$$

N would be the cation quantity within the unit cell. V would be the cell's capacity. x_c would be the critical dosage. N=3 and V=274.87 3 in this instance. The Rc value for the replacement of Tb^{3+} at the La^{3+} location is ~10.53. With $LaBSiO_5$:Tb^{3+} phosphor, energy transmission among Tb^{3+} ions are thought to predominate.

The stimulation and emitting spectra for $La_{1-y}BSiO_5$:yCe^{3+} will be displayed. These phosphors' stimulation spectra on 376 nm are emitting monitoring. The *4f-5d* shift for Ce^{3+} result in three wide stimulation bands at ~240, ~270, and ~330 nm. The stimulation strength is greatest when Ce^{3+} concentration is 0.03. Under 330 nm stimulation, the emitting spectra for $La_{1-y}BSiO_5$:yCe^{3+} are seen. These phosphors exhibit two large, overlapping peaks with about identical intensities, one at ~376 nm and the other at ~355 nm. The Ce^{3+} transitions at $5d$-$^2F_{5/2}$ and $5d$-$^2F_{7/2}$ is responsible for the two wide emitting peaks. When the $La_{0.60}BSiO_5$:$0.15Tb^{3+}$,$0.25Ce^{3+}$ excitation as well as discharge spectra are shown, it shares a similar stimulation spectrum with $La_{0.97}BSiO_5$:$0.03Ce^{3+}$. The stimulation band for Ce^{3+} overlaps the *4f-5d* conversion for Tb^{3+} between 250 and 300 nm, and there would be no evidence for the *4f-4f* conversions from 300 to 390 nm. Based on the research published by Sun *et al*, [19] this outcome was obtained. It is possible to see the radiation of Ce^{3+} and Tb^{3+} generated by the emitting spectra for $La_{0.60}BSiO_5$:0.15Tb^{3+},0.25Ce^{3+} beneath 330 nm stimulation [20]. The wide line between 360 and 420 nm would be caused by the Tb^{3+} $^5D_4 \rightarrow ^7F_J$ conversions, whereas the sequence of sharp apexes under 492, 544, 587, as well as 621 nm would be caused by the Ce^{3+} $5D$-$^2F_{7/2}$ transitions (J=6, 5, 4 and 3, respectively). The findings imply that power is transferred between Ce^{3+} and Tb^{3+}.

Schematic representation for the power shift mechanism between Ce^{3+} and Tb^{3+}. The electrons for Ce^{3+} would be stimulated between the ground status 4f and the stimulated status 5d when Ce^{3+} is exposed to UV radiation. The power would be transmitted between the 5d status for Ce^{3+} and the $^5D_{3,4}$ statuses for Tb^{3+} since it is near to the ^5D_J level. Eventually, level $^5D_{3,4}$ can emit Tb^{3+} strongly ($^5D_4$–^7F_J).

3. RESULTS AND ANALYSIS

As shown in Figure 1, the concentration of yellow phosphorus, YAG:Ce^{3+}, changed in the opposite direction to that of green phosphorus, $LaBSiO_5$:Tb^{3+}, Ce^{3+}. This adjustment has two implications: maintain mean correlated color temperature (CCT) degrees and modify how two phosphor layers in white light-emitting diodes (WLEDs) absorb and scatter light [21]. This eventually affects the color accuracy and luminous flux performance of WLEDs. The $LaBSiO_5$:Tb^{3+}, Ce^{3+} concentration chosen thus determines the color quality of WLEDs. The YAG:Ce^{3+} concentration decreased to maintain the average CCTs while the $LaBSiO_5$:Tb^{3+}, Ce^{3+} presence escalated (2-20% wt). The same is true for WLEDs, which are subjected to the scope of 5,600-8,500 K.

Figure 2 clearly illustrates the way the quantity of green phosphorus $LaBSiO_5$:Tb^{3+}, Ce^{3+} affects the discharge spectrum for WLED apparatus. High color grade apparatuses might modestly lower their lumen [22]. As seen via Figure 2, white ray would be a synthesis of the spectrum range. The images exhibit spectra at different temperatures of 5,600 K, 6,600 K, 7,000 K, 7,700 K, along with 8,500 K. The potency of two portions for the spectrum, 420–480 nm along with 500–640 nm, increases with $LaBSiO_5$:Tb^{3+}, Ce^{3+} concentration. This expansion of the two-band emission spectrum indicates an expansion of the luminous flux at the output. Additionally, the WLEDs' greater blue-light scattering suggests that both the phosphorous layer and the WLEDs' higher scattering promote color homogeneity. This outcome from the application of $LaBSiO_5$:Tb^{3+}, Ce^{3+} is significant. Controlling the hue stability for the distant phosphor formation under big heat levels may be complicated. Our investigation shows that $LaBSiO_5$:Tb^{3+}, Ce^{3+} may bring about superior hue outcome for WLED apparatuses under 5,600 as well as 8,500 K.

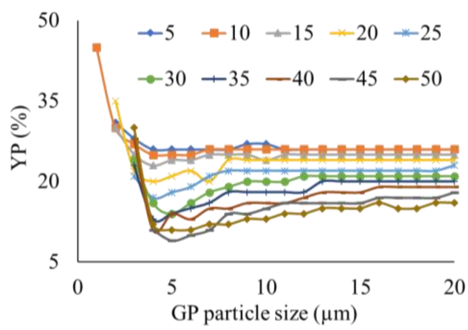

Figure 1. Retaining median CCT through altering phosphor presence

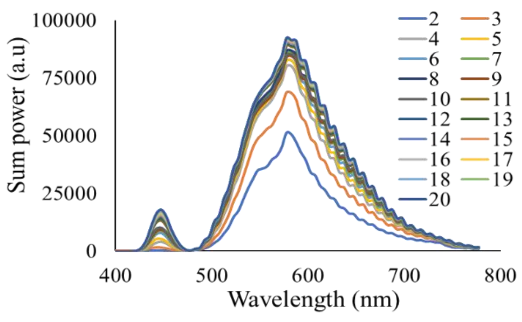

Figure 2. The discharge spectra for WLED device under 3,000 K correlating with $LaBSiO_5$:Tb^{3+}, Ce^{3+} presence

Thus, the article has demonstrated the effectiveness of the distant phosphor layer's dual-layer emission of light flux. In instance, the findings in Figure 3 demonstrate that when $LaBSiO_5:Tb^{3+}$, Ce^{3+} concentration rose from 2% weight to 20% weight, the luminous flux radiated dramatically increased. Figure 4 findings show that in all three average CCTs, the phosphor $LaBSiO_5:Tb^{3+}$, Ce^{3+} concentration greatly decreased the color deviation, which is possibly the result of the red phosphor sheet's absorption. When the $LaBSiO_5:Tb^{3+}$, Ce^{3+} phosphor absorbs the blue light generated by the light emitting diode (LED) chip, the phosphor converts it, which becomes green ray, which is then produced by the blue phosphor particles. The LED chip's blue ray would be not the only ray that the $LaBSiO_5:Tb^{3+}$, Ce^{3+} particles are able to absorb; yellow light is also absorbed. However, with the sample's assimilation features, said blue ray absorbs more blue ray compared to the two absorbs. It can be assumed that $LaBSiO_5:Tb^{3+}$, Ce^{3+} increases the amount of green light in WLEDs, which boosts the color uniformity index. Color uniformity is one of the important characteristics for contemporary WLED lamps. Obviously, the price of WLED white light increases with color homogeneity index. However, the cheap cost of $LaBSiO_5:Tb^{3+}$, Ce^{3+} is a benefit. $LaBSiO_5:Tb^{3+}$, Ce^{3+} is hence broadly applicable.

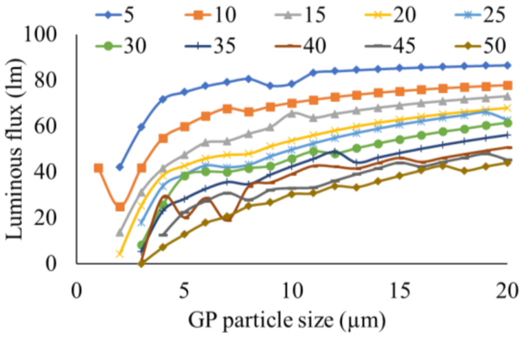

Figure 3. The lumen in WLED apparatus correlating with $LaBSiO_5:Tb^{3+}$, Ce^{3+} presence

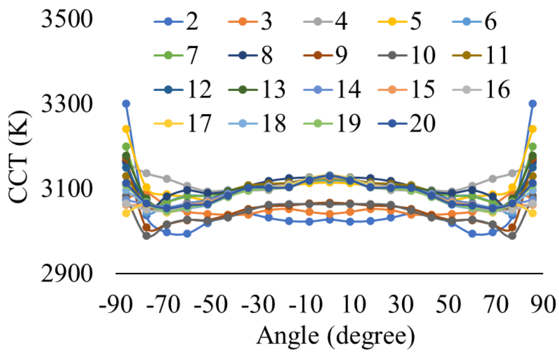

Figure 4. The CCT in WLED apparatus correlating with $LaBSiO_5:Tb^{3+}$, Ce^{3+} presence

Color uniformity would be just one aspect to consider when assessing the WLEDs' color quality [23]. Beneficial hue outcome does not depend on hue stability alone. As a result, current research works offer a scale for color quality (CQS) and an index for color rendering (CRI). CRI exhibits an entity's actual chroma when it becomes lit through light. Between the three primary hues of blue, yellow, and green, there is too much green light, which throws the color scale out of balance. This affects the hue accuracy for WLED apparatuses, causing a reduction for hue quality [24]–[26]. Figure 5 exhibits one small CRI drop when the distant phosphor $LaBSiO_5:Tb^{3+}$, Ce^{3+} sheet exists, which is an acceptable downside. CQS becomes more crucial as well as challenging to acquire if compared to CRI. Three elements influence the CQS index: CRI, watcher's choice, as well as color coordinate. As such, CQS would be virtually a universal gauging factor for color quality. Figure 6 exhibits how CQS is enhanced when the phosphor $LaBSiO_5:Tb^{3+}$, Ce^{3+} layer is present. Additionally, the concentration of $LaBSiO_5:Tb^{3+}$, Ce^{3+} does not significantly affect CQS when it is raised as the content goes below 10% wt. The substantial hue waste in the case of green becoming dominant causes CRI and CQS to shrink considerably at concentrations of $LaBSiO_5:Tb^{3+}$, Ce^{3+} more than 10% wt. As a result, choosing an appropriate concentration is crucial when using the green phosphor $LaBSiO_5:Tb^{3+}$, Ce^{3+}.

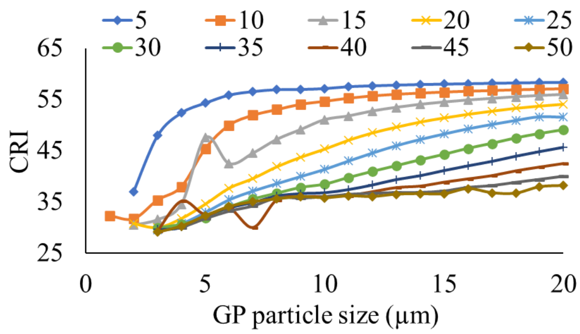

Figure 5. The CRI in WLED apparatus correlating with $LaBSiO_5:Tb^{3+}$, Ce^{3+} presence

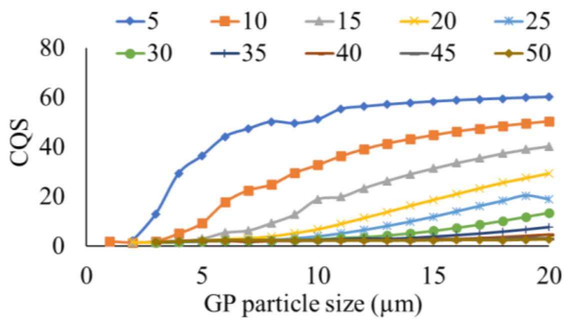

Figure 6. The CQS in WLED apparatus correlating with $LaBSiO_5:Tb^{3+}$, Ce^{3+} presence

4. CONCLUSION

The solid state technique was used to manufacture LBS doped with Ce^{3+} and Tb^{3+} at 1,100 °C. Underneath UV light stimulation, the phosphor $LBS:Tb^{3+}$ emits a strong green illumination, while $LBS:Ce^{3+}$ emits a blue-violet illumination. The green radiation from $LBS:Tb^{3+}$, Ce^{3+} got improved by the doping of Ce^{3+}. The mechanism for power shift between Ce^{3+} and Tb^{3+} is explored. Ce^{3+} is capable of effectively absorbing UV ray as well as transferring the power towards Tb^{3+}.

REFERENCES

[1] P.-P. Li *et al.*, "Unveiling of control on the polarization of supercontinuum spectra based on ultrafast birefringence induced by filamentation," *Journal of the Optical Society of America B*, vol. 35, no. 11, pp. 2916–2922, Nov. 2018, doi: 10.1364/JOSAB.35.002916.

[2] G. Granet and J. Bischoff, "Matched coordinates for the analysis of 1D gratings," *Journal of the Optical Society of America A*, vol. 38, no. 6, pp. 790–798, Jun. 2021, doi: 10.1364/JOSAA.422374.

[3] G. Prabhakar, P. Gregg, L. Rishoj, P. Kristensen, and S. Ramachandran, "Octave-wide supercontinuum generation of light-carrying orbital angular momentum," *Optics Express*, vol. 27, no. 8, pp. 11547–11556, Apr. 2019, doi: 10.1364/OE.27.011547.

[4] X. Fu *et al.*, "Micromachined extrinsic Fabry-Pérot cavity for low-frequency acoustic wave sensing," *Optics Express*, vol. 27, no. 17, pp. 24300–24310, Aug. 2019, doi: 10.1364/OE.27.024300.

[5] A. S. Baslamisli and T. Gevers, "Invariant descriptors for intrinsic reflectance optimization," *Journal of the Optical Society of America A*, vol. 38, no. 6, pp. 887–896, Jun. 2021, doi: 10.1364/JOSAA.414682.

[6] X. Yuan *et al.*, "Ultra-high capacity for three-dimensional optical data storage inside transparent fluorescent tape," *Optics Letters*, vol. 45, no. 6, pp. 1535–1538, Mar. 2020, doi: 10.1364/OL.387278.

[7] M. E. Kandel, W. Lu, J. Liang, O. Aydin, T. A. Saif, and G. Popescu, "Cell-to-cell influence on growth in large populations," *Biomedical Optics Express*, vol. 10, no. 9, pp. 4664–4675, Sep. 2019, doi: 10.1364/BOE.10.004664.

[8] S. G. Bugoffa and M. R. Chatterjee, "Electromagnetic and imaging properties of chiral dispersive spherical interfaces under bimodal propagation using ABCD matrices," *Applied Optics*, vol. 60, no. 25, pp. 7804–7814, Sep. 2021, doi: 10.1364/AO.426895.

[9] X. Sun, D. Zou, Z. Qu, and I. B. Djordjevic, "Run-time reconfigurable adaptive LDPC coding for optical channels," *Optics Express*, vol. 26, no. 22, pp. 29319–29329, Oct. 2018, doi: 10.1364/OE.26.029319.

[10] H. Nguyen, I. Misbah, and W.-C. Shih, "Smartphone sensing of multiple heavy metal ion contaminants in drinking water," in *Optical Sensors and Sensing Congress*, 2020, p. EW3H.4, doi: 10.1364/ES.2020.EW3H.4.

[11] Z. Song, Z. Song, J. Zhao, and F. Gu, "Micrometer-level 3D measurement techniques in complex scenes based on stripe-structured light and photometric stereo," *Optics Express*, vol. 28, no. 22, pp. 32978–33001, Oct. 2020, doi: 10.1364/OE.401850.

[12] D. M. Kustov *et al.*, "Laser-induced fluorescent visualization and photodynamic therapy in surgical treatment of glial brain tumors," *Biomedical Optics Express*, vol. 12, no. 3, pp. 1761–1773, Mar. 2021, doi: 10.1364/BOE.415936.

[13] H. Jia *et al.*, "High-transmission polarization-dependent active plasmonic color filters," *Applied Optics*, vol. 58, no. 3, pp. 704–

711, Jan. 2019, doi: 10.1364/AO.58.000704.
[14] H. Cheng, S. Tong, X. Deng, J. Li, P. Qiu, and K. Wang, "In vivo deep-brain imaging of microglia enabled by three-photon fluorescence microscopy," *Optics Letters*, vol. 45, no. 18, pp. 5271–5274, Sep. 2020, doi: 10.1364/OL.408329.
[15] W.-Y. Chang, Y. Kuo, Y.-W. Kiang, and C. C. Yang, "Simulation study on light color conversion enhancement through surface plasmon coupling," *Optics Express*, vol. 27, no. 12, pp. 629–642, Jun. 2019, doi: 10.1364/OE.27.00A629.
[16] R. Deeb, J. V. de Weijer, D. Muselet, M. Hebert, and A. Tremeau, "Deep spectral reflectance and illuminant estimation from self-interreflections," *Journal of the Optical Society of America A*, vol. 36, no. 1, pp. 105–114, Jan. 2019, doi: 10.1364/JOSAA.36.000105.
[17] S. An, J. Li, X. Li, and Y. Su, "FTN SSB 16-QAM signal transmission and direct detection based on tomlinson-harashima precoding with computed coefficients," *Journal of Lightwave Technology*, vol. 39, no. 7, pp. 2059–2066, Apr. 2021, doi: 10.1109/JLT.2020.3046717.
[18] K. Orzechowski, M. M. Sala-Tefelska, M. W. Sierakowski, T. R. Woliński, O. Strzeżysz, and P. Kula, "Optical properties of cubic blue phase liquid crystal in photonic microstructures," *Optics Express*, vol. 27, no. 10, pp. 14270–14282, May 2019, doi: 10.1364/OE.27.014270.
[19] J. Sun, J. Lai, Z. Xia, X. Zhang, H. Liu, and H. Du, "Luminescence properties and energy transfer in Ba2Y(BO3)2Cl:Ce3+,Tb3+ phosphors," *Applied Physics B*, vol. 107, no. 3, pp. 827–831, Jun. 2012, doi: 10.1007/s00340-012-4961-5.
[20] S. Ma, P. Hanselaer, K. Teunissen, and K. A. G. Smet, "Effect of adapting field size on chromatic adaptation," *Optics Express*, vol. 28, no. 12, pp. 17266–17285, Jun. 2020, doi: 10.1364/OE.392844.
[21] C. McDonnell, E. Coyne, and G. M. O'Connor, "Grey-scale silicon diffractive optics for selective laser ablation of thin conductive films," *Applied Optics*, vol. 57, no. 24, pp. 6966–6970, Aug. 2018, doi: 10.1364/AO.57.006966.
[22] K. Liu and Y. Liang, "Underwater image enhancement method based on adaptive attenuation-curve prior," *Optics Express*, vol. 29, no. 7, pp. 10321–10345, Mar. 2021, doi: 10.1364/OE.413164.
[23] T. Shang, Z. P. Sun, Z. Y. Dong, and Q. Li, "Network selection method based on MADM and VH-based multi-user access scheme for indoor VLC hybrid networks," *Optics Express*, vol. 26, no. 23, pp. 30795–30817, Nov. 2018, doi: 10.1364/OE.26.030795.
[24] S. Bernard, T. J. Clark, V. Dumont, J. Ma, and J. C. Sankey, "Monitored wet-etch removal of individual dielectric layers from high-finesse Bragg mirrors," *Optics Express*, vol. 28, no. 23, pp. 33823–33829, Nov. 2020, doi: 10.1364/OE.400986.
[25] C. J. C. Smyth, S. Mirkhanov, A. H. Quarterman, and K. G. Wilcox, "275 W/m 2 collection efficiency solar laser using a diffuse scattering cooling liquid," *Applied Optics*, vol. 57, no. 15, pp. 4008–4012, May 2018, doi: 10.1364/AO.57.004008.
[26] S. Yuan *et al.*, "Enhanced nonlinearity for filamentation in gold-nanoparticle-doped water," *Chinese Optics Letters*, vol. 17, no. 3, pp. 1–5, 2019, doi: 10.3788/COL201917.032601.

BIOGRAPHIES OF AUTHORS

Ha Thanh Tung received the Ph.D degree in physics from University of Science, Vietnam National University Ho Chi Minh City, Vietnam, he is working as a lecturer at the Faculty of Basic Sciences, Vinh Long University of Technology Education, Vietnam. His research interests focus on developing the patterned substrate with micro and nano scale to apply for physical and chemical devices such as solar cells, OLED, and photoanode. He can be contacted at email: tunght@vlute.edu.vn.

Huu Phuc Dang received a Physics Ph.D degree from the University of Science, Ho Chi Minh City, in 2018. Currently, he is a lecturer at the Faculty of Fundamental Science, Industrial University of Ho Chi Minh City, Ho Chi Minh City, Vietnam. His research interests include simulation LEDs material and renewable energy. He can be contacted at email: danghuuphuc@iuh.edu.vn.

Phung Ton That was born in Thua Thien-Hue, Vietnam. He received the B.Sc. degree in electronics and telecommunications engineering (2007) and the M.Sc. degree in electronics engineering (2010) from the University of Technology, Vietnam. He is currently a lecturer at the Faculty of Electronics Technology (FET), Industrial University of Ho Chi Minh City. His research interests are optical materials, wireless communication in 5G, energy harvesting, performance of cognitive radio, physical layer security, and NOMA. He can be contacted at email: tonthatphung@iuh.edu.vn.